 FDMP, vol.1, no.2, pp.189-199, 2005

Liquid Particles Tracing in Three-dimensional Buoyancy-driven Flows

D. E. Melnikov[1] **and V. M. Shevtsova**[2]

Abstract: Buoyancy-driven convective flows are numerically analyzed in a cubic enclosure, containing a liquid subjected to a temperature difference between opposite lateral walls; all other walls are thermally insulated. The stationary gravity vector is perpendicular to the applied temperature gradient. The steady flow patterns are investigated within the framework of a liquid particles tracing technique. Three tracing techniques are compared: the first, based on a trilinear interpolation of the liquid velocity defined on the computational grid and an eighth order in time Runge-Kutta method; the second and the third, using a resampling the velocity field on a new approximately twice finer grid by cubic spline interpolation and then a combination of trilinear interpolation of velocity on the new grid, integrating in time with (2-nd method) a single forward time marching method; (3-rd method) a fourth order Runge-Kutta algorithm. Comparison of the results shows that for obtaining a precise tracing on a long time scale it is more important to have a good spatial velocity accuracy than precise integration in time. Unlike one vortex 2D pattern where the particles follow thin and closed circle trajectories staying in vertical cross-sections, it is shown that,the 3D flow consists of two sets of spiral-type motions identical in both halves of the cell with respect to the mid-plane. In the 3D flow even in the central vertical cross-section the particles follow spiral non-closed trajectories drifting outward the cube's walls. It demonstrates that two-dimensional approach does not provide a clear picture of 3D convection.

keyword: Particle tracing, convective flow, buoyancy.

1 Introduction

The experimental and theoretical determination of the flow structure is very important in many fluid mechanics studies. A few visualization techniques are applicable to observe internal behavior of fluid in experiments. A common experimental approach is the tracing of small particles initially injected into the media. Among the requirements to the particles incorporated into the liquid is that they should not influence much the flow itself and alter the properties of the system.

Flow imaging can be made by different techniques. Among the well known and highly utilized are those using Particle Image Velocimetry (PIV) [Raffel, Willert, and Kompenhaus (1997)], radiographic techniques [Blet, Berne, Chaussy, Perrin, and Schweich (1999)]. Various optical methods such as interferometry, schlieren and shadowgraph techniques can give the general structure of the flow. The PIV visualizes fluid motion using tracer particles having different optical properties than the fluid. It is applied mostly for physical studies in transparent fluids [Hiller, Koch, Kowalewski, and Stella (1993)]. By this method, two or three dimensional velocity field distributions can be obtained. Usually, the approach requires seeding the flow with small tracer particles and illuminating with a sheet or volume of light originated from a pulsed laser. A single or multi-exposure image of the position of the particles as a function of time is recorded. The spacing between these particle images provides a measure of the local flow velocity.

The radiography is based on either detecting the difference of material density of the particles-fluid system or tracking radioactive materials. The use of radiography for visualization of the process is usual in clinical studies or when the media is optically opaque, e.g. when a radiographic contrast material is injected into the blood for quantifying its regional flow [Tarver and Plant (1995)].

A detailed discussion of the experimental techniques is beyond the scope of the study, that is focused visualization of computational fluid dynamics results. A meaningful visualization of the data is required in many circumstances to understand the characteristics of the simulated process. A review with multiple examples on the visualization of numerical results can be found e.g. in [Post and Walsum (1993)].

The classical Navier-Stokes equations, the basic of the CFD, have been extensively studied for many years and

[1] ULB, Brussels, Belgium.

different numerical approaches for solving them have been developed. Two main descriptions of fluid dynamics may be distinguished: Eulerian and Lagrangian. Each approach has its issues, results in a particular form of the Navier-Stokes equations and thus is more suitable for certain types of problems.

The Lagrangian approach is more adequate for the particle tracing. In the Lagrangian formulation the variables are linked to the initial positions of selected particles and thus the physical quantities are given as functions of the starting positions and of time. Visualization in this case often leads to dynamic images of moving particles, showing only information in the particles locations. The trajectory of each particle is computed separately. However, one of the limitations of the Lagrangian approach is that the particles may accumulate into clusters. As a consequence, a re-meshing is needed for each time step. As alternative to this re-meshing, Smooth Particle Hydrodynamics Method was developed [Gingold and Monaghan (1977)]. It is based on Kernel approximations to interpolate the unknowns and was initially used for the treatment of astrophysical hydrodynamic problem. Using the idea of a polynomial interpolation that fits not globally the whole set but just a number of points, meshless methods have been developed [E. Oñate and S. R. Idelsohn and O. C. Zienkiewicz and R. L. Taylor(1996)]. Recently meshless methods for the particle-fluid interaction have been suggested in Finite Element Approximation [Johnson and Tezduyar (1997)].

In the Eulerian formulation the data are computed on a discrete grid, and are stored locally in selected points. Visualization tends to produce static images of the whole study area. It is not difficult to visualize scalar and one- or two-dimensional vector fields, but a clear picture of the velocity in a 3D bulk is a complicated task. So, one needs other approaches to visualize the flow.

Some intuitive methods of vector fields' visualization were suggested, e.g. for unsteady flow as a collection of streaklines [Lane (1996)] that originate from user-defined seed points, and particle tracing [G. M. Nielson and M. Magen and H. Müller(1997)]. For steady processes streamlines [Helman and Hesselink (1991)], stream surfaces [Hultquist (1990)] can be used. They are robust methods; however it becomes important to correctly seed the point into the computational domain to avoid loosing information about the field.

Gelfgat (1999) used streaklines of perturbation of velocity for visualizing the Rayleigh-Bénard convective flow in rectangular enclosures of different aspect ratios. Particularly, thin closed streaklines similar to two-dimensional convection in a square were observed in a cube. Increasing the aspect ratio led to different flow regimes with the streaklines being more complicated.

The problem of natural convection in a cube differentially heated (gravity perpendicular to the applied temperature difference) has been investigated both experimentally and numerically [Hiller, Koch, Kowalewski, de Vahl Davis, and Behnia (1990); Hiller, Koch, Kowalewski, and Stella (1993)]. They used the PIV technique for liquid-crystal tracers suspended in the flow and direct numerical simulations for solving the Navier-Stokes equations in Boussinesq approximation. A double spiral-type motion of the particles away from the central plane was observed. This proved the three-dimensionality of the flow. It was numerically shown that 2D calculations might be sufficient to describe the flow only in the center plane of the cube.

Additional techniques of flow visualization that can describe the global behavior of vector fields were suggested. Aiming at imaging a 3D vector field, [Crawfis and Max (1993)] considered direct volume rendering methods. Their idea was to construct three-dimensional scalar signals from the vector data using vector kernels and texture splats. [Cabral and Leedom (1993)] proposed a Line Integral Convolution method utilized for visualizing flows over surfaces and more recently in a 3D domain. This method uses a one-dimensional low pass filter to convolve an input texture along the principal curves of the vector field.

2 Description of the mathematical problem

The Eulerian approach, used in present study, defines the unknowns in fixed points (nodes of the computational mesh). Considered particles are iso-dense with the fluid, having no size and no forces acting on them. Such liquid particle, being seeded at a point (x_0, y_0, z_0) in the bulk, will follow exactly the flow. The starting point is usually selected by the researcher.

Below we discuss successively: (a) the problem of integrating equation of motion of a liquid particle; (b) the problem of interpolation at arbitrary points of velocity defined on a grid; (c) comparison of three numerical tracing techniques for a two-dimensional buoyancy-driven

convective flow in a square. This leads to the selection of the best method for further application to the three-dimensional problem.

2.1 Integration of the kinematic equation of particle

Here, the goal is to find how the particle's path $(x(t), y(t), z(t))$ develops over time (t is the time). Motion of a neutrally buoyant and non-diffusing particle of the liquid is given by a simple equation:

$$\frac{d\tilde{\mathbf{R}}}{dt} = \tilde{\mathbf{V}}, \quad \tilde{\mathbf{R}} = (x, y, z), \quad \tilde{\mathbf{V}} = (V_x, V_y, V_z). \tag{1}$$

where $\tilde{\mathbf{V}}$ is velocity and $\tilde{\mathbf{R}}$ is the particle's location.

In non-vector representation Eq. 1 is a system of three ordinary differential equations

$$\frac{dx}{dt} = V_x, \qquad \frac{dy}{dt} = V_y, \qquad \frac{dz}{dt} = V_z,$$

with initial conditions at time zero:

$$x(t=0) = x_0, \quad y(t=0) = y_0, \quad z(t=0) = z_0.$$

Thus, visualization of the flow consists of integrating simple Eq. 1 for a set of initial coordinates (x_0, y_0, z_0) and then drawing the resulting paths (x, y, z).

The first step in a particle tracking procedure is solving the flow equations (a system of Navier-Stokes, energy and continuity equations for the considered problem), which gives velocities at cell edges of the simulation grid. Then, knowing $\tilde{\mathbf{V}}$ the integration of Eq. 1 can be accomplished. Usually for particle tracking the first-order Euler's algorithm [Goode and Konikow (1989); Lu (1994)] and the fourth-order Runge-Kutta [Shafer (1987)] method are used. These schemes are not limited by transient velocities or complexity in the velocity field.

Euler's algorithm is computationally the simplest technique. Intuitively, the particle moves by a little step along the velocity vector to the next position. It is an explicit first-order in time method:

$$x(t+\Delta t) = x(t) + V_x \Delta t, \tag{2}$$

$$y(t+\Delta t) = y(t) + V_y \Delta t, \tag{3}$$

$$z(t+\Delta t) = z(t) + V_z \Delta t, \tag{4}$$

where Δt is the time step.

It works well in areas where the velocity fields are sufficiently uniform, like in flow through a straight channel. If the flow rapidly changes its direction or there are areas of strong converging (diverging), then the Euler's method may give a wrong picture of the liquid particles' trajectories. One can not take an arbitrary time step because of a quite severe limitation on the Δt for achieving sufficient accuracy in the particle tracing.

Another technique, which is more accurate, is the Runge-Kutta method. It can be of second, fourth order and even more accurate. The main idea of the Runge-Kutta method of the $m-th$ order is to evaluate the velocity m times to calculate the particle's position $\tilde{\mathbf{R}}(t+\Delta t)$ on the next time step. The new position of the particle is evaluated using a velocity which is a linear combination of the values at m points. For example, the Runge-Kutta process of second order may be expressed as follows:

$$\tilde{\mathbf{R}}^* = \tilde{\mathbf{R}}(t) + \tilde{\mathbf{V}}(\tilde{\mathbf{R}}(t))\Delta t, \tag{5}$$

$$\tilde{\mathbf{R}}(t+\Delta t) = \tilde{\mathbf{R}}(t) + 0.5(\tilde{\mathbf{V}}(\tilde{\mathbf{R}}(t)) + \tilde{\mathbf{V}}(\tilde{\mathbf{R}}^*))\Delta t. \tag{6}$$

The Runge-Kutta method permits using larger Δt compared to the Euler's algorithm, and this can be regarded as its most important advantage.

2.2 Interpolation of velocity

As mentioned above, the velocity values are defined on a static Eulerian mesh used for calculations. Obviously, particles' trajectories are smooth and continuous lines in space. Here a problem of interpolation of the velocity appears since one requires the evaluation of the velocity at a point which is arbitrary with respect to the nodes of the mesh. There is a large variety of velocity interpolation schemes, mostly common are multilinear (bilinear, trilinear) and splines.

Trilinear interpolation is a process of linearly interpolating points within a 3D box given the values at the vertices or at the centers of the facelets of the box. It is a widely used interpolating technique since it is fast (it is a local interpolating method) and simple and it works well on a fine mesh. The three-dimensional velocity field is computed as a weighted sum of these eight field's values in the surrounding grid points.

Spline interpolations could be more accurate than multilinear. In [Rybak and Huybrechts (2003)] a comparison between accuracies of piecewise bilinear and bi-cubic spline interpolations was considered and it was shown

that spline interpolation is at least of three orders of magnitude more accurate than bilinear. Unlike the multilinear, cubic-spline interpolation is not a local interpolation as it requires knowledge of the velocity values in a model subdomain. Numerically it is a time-consuming method.

3 Formulation of the physical problem

Three-dimensional natural convection is considered in a cubic cell of size L with differentially heated opposite vertical walls. The temperatures T_{hot} and T_{cold} ($T_{hot} > T_{cold}$) are prescribed at the right and left boundaries respectively, yielding a temperature difference of $\Delta T = T_{hot} - T_{cold}$. All other walls are assumed to be thermally insulated. Geometry of the problem is shown in Fig. 1.

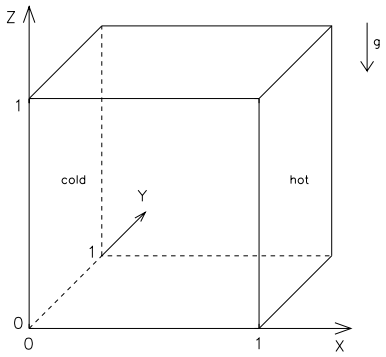

Figure 1 : Problem's geometry: cube heated from side

The governing Navier-Stokes, energy and continuity equations are written in non-dimensional primitive-variable formulation.

$$\frac{\partial \tilde{\mathbf{V}}}{\partial t} + \tilde{\mathbf{V}} \cdot \nabla \tilde{\mathbf{V}} = -\nabla P + \nabla^2 \tilde{\mathbf{V}} + Gr \Theta \tilde{\mathbf{e}}, \tag{7}$$

$$\nabla \cdot \tilde{\mathbf{V}} = 0, \tag{8}$$

$$\frac{\partial \Theta}{\partial t} + \tilde{\mathbf{V}} \cdot \nabla \Theta = \frac{1}{Pr} \cdot \nabla^2 \Theta, \tag{9}$$

where velocity is defined as $\tilde{\mathbf{V}} = (V_x, V_y, V_z)$, $\Theta = (T - T_{cold})/\Delta T$ is the dimensionless temperature. The equations have been nondimensionalized by using L as the length scale. Velocity and time are scaled by ν/L and L^2/ν (ν is the kinematic viscosity). P is dimensionless pressure. $\tilde{\mathbf{e}}$ is a unit vector parallel to the gravity acceleration vector $\tilde{\mathbf{g}}$.

The operator

$$\nabla = \frac{\partial}{\partial x}\tilde{\mathbf{e}_x} + \frac{\partial}{\partial y}\tilde{\mathbf{e}_y} + \frac{\partial}{\partial z}\tilde{\mathbf{e}_z}$$

At the rigid walls no slip conditions are imposed:
$\tilde{\mathbf{V}}(x=0,y,z,t) = 0,\ \tilde{\mathbf{V}}(x=1,y,z,t) = 0,$
$\tilde{\mathbf{V}}(x,y=0,z,t) = 0,\ \tilde{\mathbf{V}}(x,y=1,z,t) = 0,$
$\tilde{\mathbf{V}}(x,y,z=0,t) = 0,\ \tilde{\mathbf{V}}(x,y,z=1,t) = 0.$
Boundary conditions for temperature are the following:
$\Theta(x=0,y,z,t) = 0,\ \Theta(x=1,y,z,t) = 1,$
$\frac{\partial \Theta}{\partial y}(x,y=0,z,t) = 0,\ \frac{\partial \Theta}{\partial y}(x,y=1,z,t) = 0,$
$\frac{\partial \Theta}{\partial z}(x,y,z=0,t) = 0,\ \frac{\partial \Theta}{\partial z}(x,y,z=1,t) = 0.$

The formulation of the problem includes Prandtl and Grashof numbers:

$$Pr = \frac{\nu}{\alpha},\ \ Gr = \frac{g\beta_T \Delta T L^3}{\nu^2},$$

where α is the thermal diffusion coefficient and β_T is the thermal expansion coefficient. The study below is given for the following parameters: $Pr = 7, Gr = 150$.

4 Numerical technique

A finite volume technique based on an explicit single time step marching method is employed. The computational domain is discretized by a staggered uniform mesh in all three directions. All the scalar variables (P, Θ) are defined in the centers of the grid cells while the velocity values are stored in centers of the cells' facelets. Central differences for spatial derivatives and forward differences in time are employed. Numerical steady state solutions are obtained by convergence of the transient calculations. Computation of the velocity field at each time step is carried out by a projection method, see e.g. [Fletcher (1988)]. A combination of fast Fourier transforms in the $Y-$direction and an implicit ADI method in the two others is applied for solving the Poisson equation for the pressure. A more detailed description and validation of the numerical code is given in [Shevtsova, Melnikov, and Legros (2001); Shevtsova, Melnikov, and Legros (2004)].

The results of this paper were obtained on a mesh $(25 \times 32 \times 30)$. This grid was shown to be sufficient for modeling the natural convection in enclosures at moderate Grashof numbers [Shevtsova, Melnikov, and Legros (2004)].

5 Results

A non-uniform density distribution occurs in the cell when heated from a side in the presence of gravity and $\Delta T \neq 0$. Near the hot wall, the density is less than near the cold one. As a result, the denser liquid flows downward along the cold wall and the lighter flows upward. Due to the presence of the lateral walls, a vortex-type stationary flow will be observed.

5.1 Pseudo 2D problem calculated by 3D code

Hereafter, the unphysical two-dimensional flow pattern provided by 3D simulations in which the velocity component V_y is always kept equal to zero ($V_y = 0$) is referred to as "pseudo two-dimensional flow". It is used as a reliable test problem before starting dealing with fully three-dimensional particle tracing. It cannot be regarded as the classical 2D case since there are lateral walls bounding the viscous flow in y-direction, $V_x = V_z = 0$ at $y = 0, 1$. Thus a well-known two-dimensional flow is established in the middle of the cube $y = 0.5$ and some deviations with respect to this flow occur close to the walls. At moderate ΔT the flow pattern consists of only one vortex in the $XZ-$section with its center in the middle of the domain. A liquid particle will follow concentric closed streamlines, see Fig. 2.

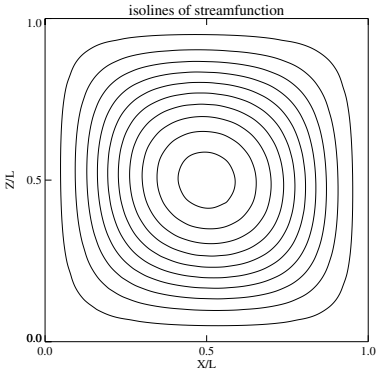

Figure 2 : Lines of constant values of stream function calculated for the 2D case ($V_y = 0$) in $Y = 0.5$ mid-plane

The particles tracing technique includes two aspects: calculation of the velocity in the location point of the particle, and integration of Eq. 1. We compared results of tracing obtained by the following algorithms:

Method 1. Trilinear velocity interpolation is applied on the computational grid $(25 \times 31 \times 30)$. Integration in time is based on eighth order Runge-Kutta algorithm, which is of the eighth order accuracy in time.

Method 2. The known velocity field $\tilde{\mathbf{V}}$ is resampled on a new finer mesh $(50 \times 50 \times 50)$ by cubic spline interpolation. Trilinear velocity interpolation is applied on this new grid. The single time step marching method is used for the integration in time. This is a first order accurate in time method.

Method 3. The known velocity field $\tilde{\mathbf{V}}$ is resampled on a new finer mesh $(50 \times 50 \times 50)$ by cubic spline interpolation. Trilinear velocity interpolation is applied on the new grid. Integration in time is based on fourth order Runge-Kutta algorithm, which is of the fourth order accuracy in time.

The three tracing techniques used for this study are shown in Fig. 3.

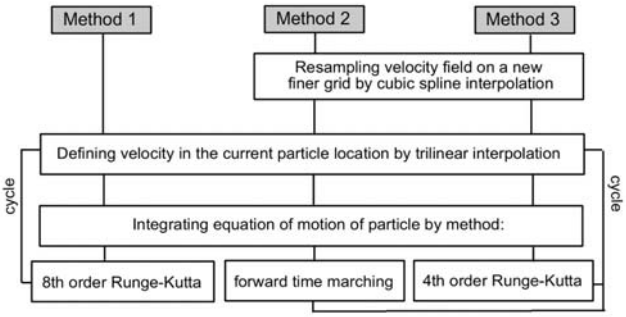

Figure 3 : Schematic diagram representing the three methods of tracing

Fig. 4 represents a comparison between the three methods. Three particles were placed inside the bulk with initial coordinates: $(0.2, 0.2, 0.2)$, $(0.2, 0.5, 0.2)$ and $(0.2, 0.8, 0.2)$. The tracing time step Δt is equal to 10^{-3}. Similar to the two-dimensional convection in a square, in the considered case the flow pattern is a set of vortexes parallel to the $XZ-$plane with vorticity changing as a function of Y; the maximum is in the mid-plane and drops down to zero on the rigid walls.

Method 3 gives the best result, i.e. thin closed trajectories for all the particles (Fig. 4(c)) and it is just slightly more time-consuming than Method 2. The trajectories by Method 2 also look good, but the traces calculated by Method 1 (Fig. 4(a)) are not thin and closed, especially for the second particle placed in the $Y = 0.5$ mid-plane, the region of the largest velocities. The particles' traces

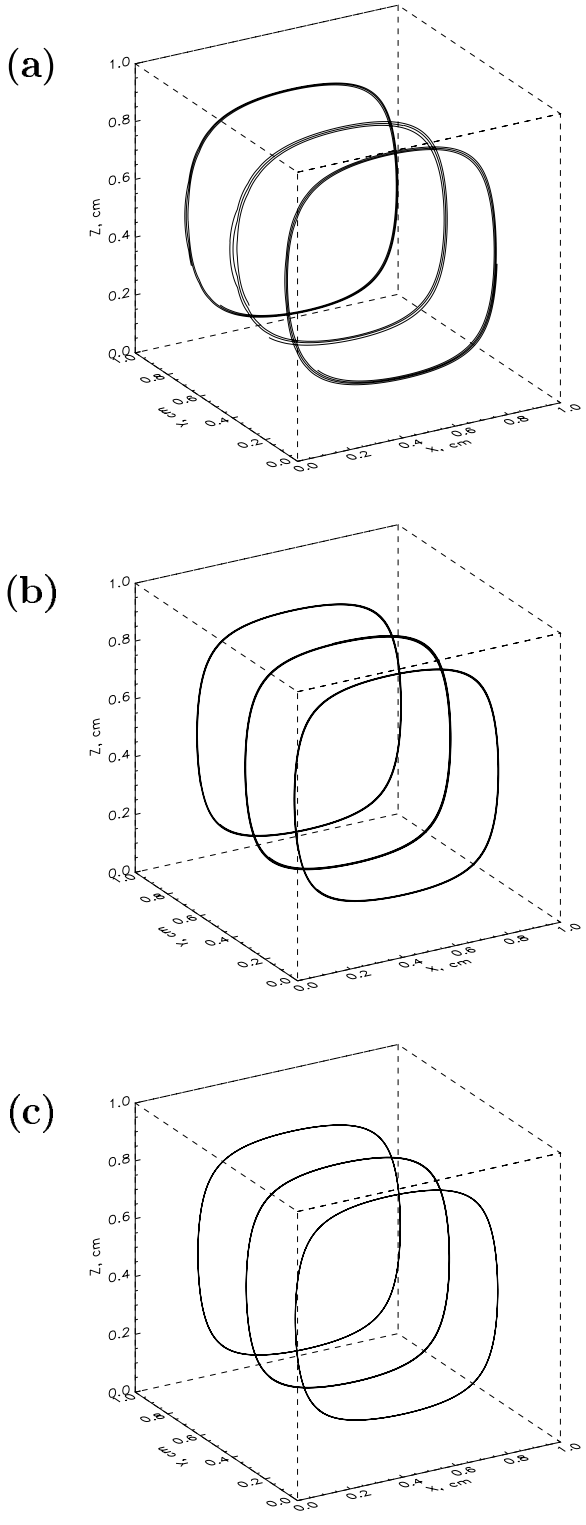

Figure 4 : Three liquid particles' trajectories traced for the *pseudo* 2D case ($V_y = 0$) by the three techniques: (a) **Method 1**; (b) **Method 2**; (c) **Method 3**. Initial points are $(x_0, y_0, z_0) = (0.2, 0.2, 0.2)$, $(0.2, 0.5, 0.2)$, $(0.2, 0.8, 0.2)$

calculated by the Method 1 exhibit a tendency to diverge toward either the center (as if there was a sink in the center) or the walls (as if there was a source in the center), depending on value of Δt. When $\Delta t = 10^{-3}$, this trajectory slowly diverges toward the cell's center (Fig. 5(a)). Taking $\Delta t = 10^{-2}$, the trajectories are pushed outwards (Fig. 5(b)). All these features point out that Method 1 is not appropriate for this kind of investigation.

To summarize, Method 1 is affected by an instability and is not suitable for precise tracing, even if it uses the eighth order Runge-Kutta algorithm. A more precise spatial velocity interpolation is needed than that related to Method 1. The thinnest closed trajectories are obtained using Method 3, which is quite fast and robust. Since the two methods use velocity approximations on grid with different resolutions, the latter becomes a key point for a good tracing. Even the single forward time-marching procedure of Method 2 is able to give a good result if the velocity is accurately interpolated (Fig. 4(b)).

5.2 Fully 3D problem

The three-dimensional effects for the buoyancy-driven convection flow in differentially heated enclosures were discussed earlier, see e.g. [Davis (1967)]. It was argued that a secondary flow with a velocity component parallel to the roll axis appears due to the interaction of the main circulation roll with the side walls. In [Mallinson and de Vahl Davis (1977)] it was numerically predicted that toroidal circulation cells occur in enclosures with different aspect ratios, Prandtl and Rayleigh numbers. This flow is generally directed toward the mid-plane in the center and outwards at the periphery.

In the fully 3D problem of natural convection in a cube the velocity $V_y \neq 0$. Though its calculated value for the present conditions ($Pr = 7$, $Gr = 150$) is small, $max(|V_y|)/max(|V|) = 0.016$, the three-dimensional flow pattern is different with respect to the two-dimensional test considered above. As in the $Y = 0.5$ central section $V_y = 0$, liquid particles, being initially there, should always stay in this cross-section. One could expect in this region thin closed trajectories (similar to the ones of Fig. 4(b),(c)). But it appears to be not so. The trajectories calculated using the Methods 1, 2 and 3 with $\Delta t < 10^{-3}$ for the particle initially placed at $(x_0, y_0, z_0) = (0.2, 0.5, 0.2)$ are depicted in Fig. 6. The trajectories obtained by the accurate Methods 2 and 3 (Fig. 6(b),(c)) look very similar. The particle tends to drift toward the

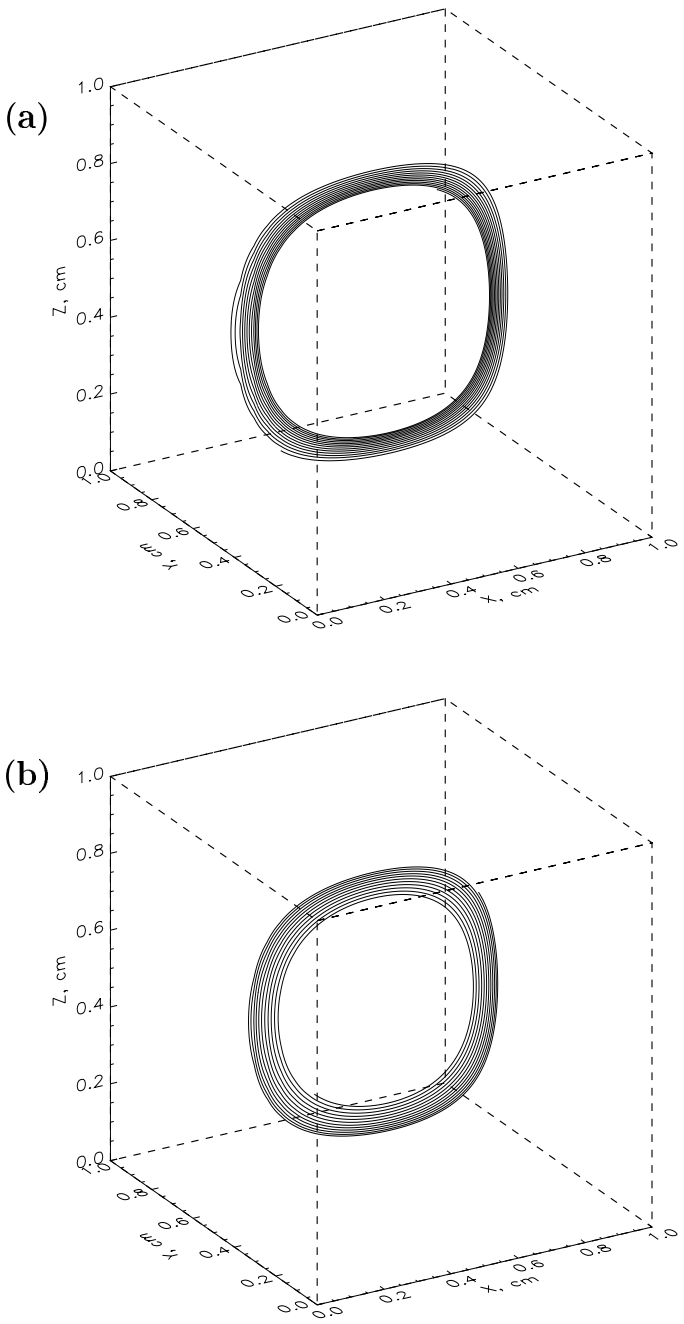

Figure 5 : Non-closed liquid particles' trajectories traced for the *pseudo* 2D case ($V_y = 0$) by Method 1 with different tracing time steps: (a) starting at $(x_0, y_0, z_0) = (0.2, 0.5, 0.2)$ with $\Delta t = 10^{-3}$ trajectory goes toward the cell's center; (b) when $\Delta t = 10^{-2}$ and $(x_0, y_0, z_0) = (0.3, 0.5, 0.3)$, trajectory diverges outwards

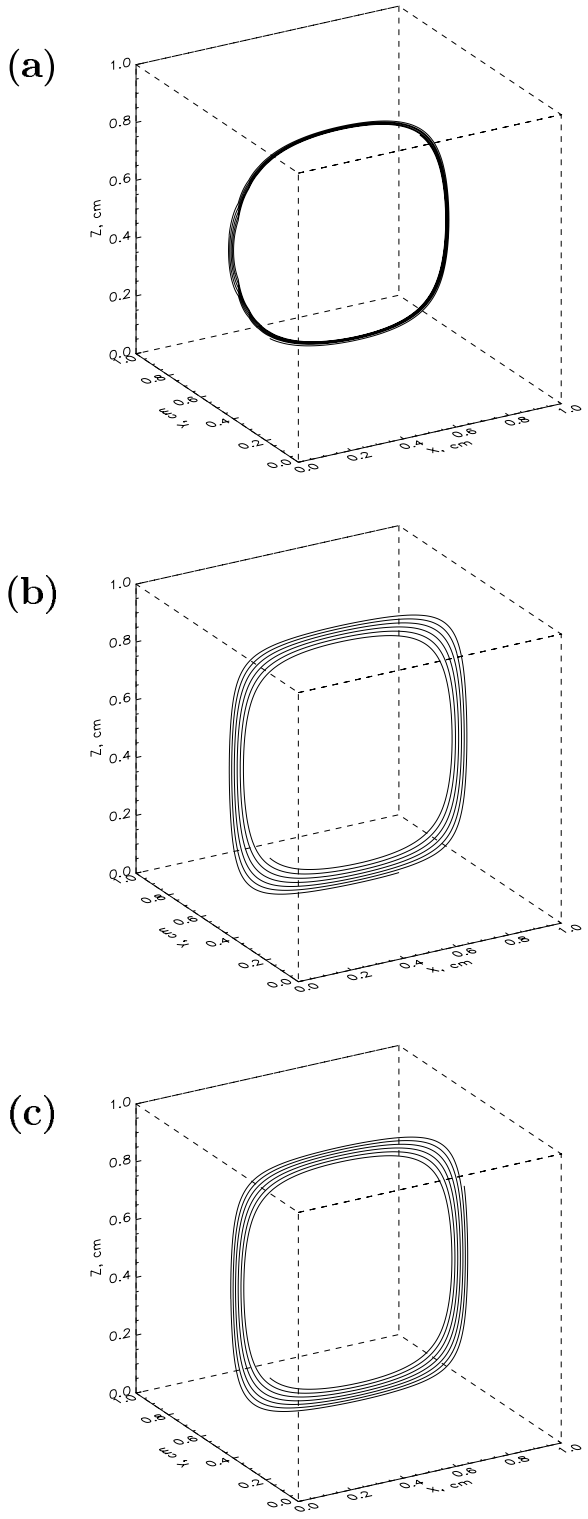

Figure 6 : Liquid particle's trajectories in the central cross-section $Y = 0.5$ traced for the 3D case by the three techniques: (a) Method 1; (b) Method 2; (c) Method 3. Initial point $(x_0, y_0, z_0) = (0.2, 0.5, 0.2)$

walls (a source in the center). Though the particle traced by the Method 3 covers slightly longer path during the same tracing time.

However, tracing performed by Method 1 leads to completely different results. The particle is slowly drifting toward the center of the cell while following a circle trajectory (Fig. 6(a)). This must be regarded as a wrong result being a superposition of the correct drifting outward, proven by the calculations by Method 3 (Fig. 6(c)), and a numerically incorrect shifting toward the center at this tracking time step (see Fig. 5(a)) with the latter effect prevailing.

So, the correct particles' trajectories in the $Y = 0.5$ plane are the ones shown in Fig. 6(b),(c). Why are they not closed? To shed some light on the reason of such unexpected behavior of the particles, one should analyze the tracers initially put somewhere beyond the mid-plane. Fig. 7 illustrates the flow structure beyond the central plane. For better understanding, three different views of the same particle's trajectory are shown. This trajectory was computed by means of Method 3 ($N = 600000$ tracing steps with $\Delta t = 10^{-3}$, that should give almost no divergence from the "true" particle's path while integrating with the fourth-order Runge-Kutta algorithm).

The particles on the both sides with respect to the $Y = 0.5$ mid-plane follow closed spiral trajectories with symmetry axis $(0.5, Y, 0.5)$ looking like ordinary ring torii. The closer the particle is initially seeded to the side walls $Y = 0$, $Y = 1$, the slower it moves. The liquid on Fig. 7 following spiral-type trajectory flows outwards on the exterior surface of the torus and comes back along its interior surface in agreement with the earlier findings in [Mallinson and de Vahl Davis (1977)]. Since near the mid-plane $Y = 0.5$ the flow turns toward the lateral rigid wall, it evolves the fluid particles at this central plane in the same kind of movement (Fig. 6(b),(c)). It explains why the liquid particles in the full 3D problem do not make closed trajectories, i.e. the 3D problem in differentially heated cavity generally cannot be modeled by a simple 2D approach.

This difference with respect to 2D models, except in the mid-plane, has been mentioned in [Hiller, Koch, Kowalewski, de Vahl Davis, and Behnia (1990)]. It was also found that there exists a "cross-flow" from two opposite lateral walls to the cavity center consisting of spiraling motions. This motions are perpendicular to the main convective recirculation from the hot to the cold

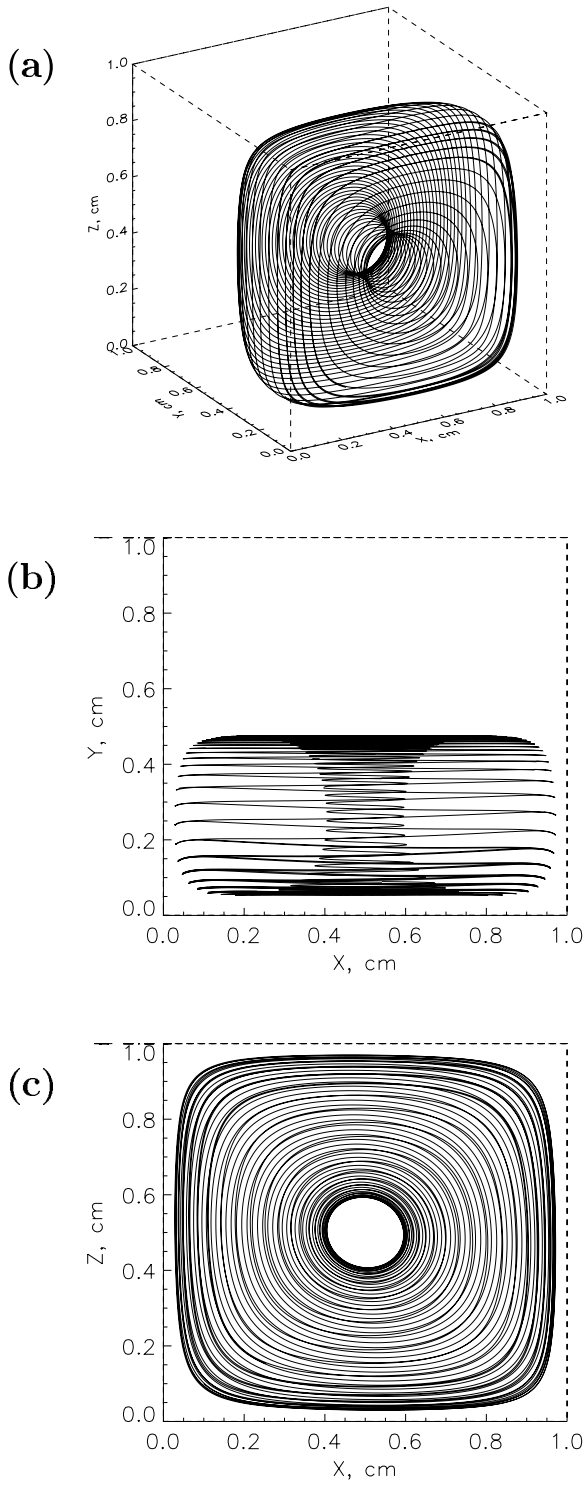

Figure 7 : Three different views of liquid particle's trajectory initially placed in point $(x_0, y_0, z_0) = (0.1, 0.2, 0.1)$. The particle makes closed torus-like trace.

wall, that is in agreement with the present simulations.

There is an aspect requiring clarification. How do particles in the mid-section leave this plane since the velocity component $V_y = 0$? In practice, getting closer to the walls, the flow slows down and in natural experiments it leaves this cross-section due to some random external flow disturbances or non-ideal internal cell's surface. However, in accurate numerical calculations such fluid particle will asymptotically approach the walls.

In addition two interesting flow regions are found:

- the symmetry axis $(0.5, Y, 0.5)$ of the spiral-type trajectories,

- set of points in $Y \approx 0.255$ and $Y \approx 0.745$ vertical planes.

Initially seeded fluid particle somewhere on the symmetry axis will be transported by the fluid toward the center of cell and will asymptotically approach it progressively slowing down (straight line on Fig. 8). The fluid initially placed in the cell's center will stuck there and will never leave it. Tracings by both Method 2 and 3 give the same result. This result was thoroughly verified by performing many tracing steps starting with different points $(0.5, y_0, 0.5)$.

Since spiral-type closed trajectories make torii-like looking surfaces, there must be a continuous set of points in two vertical planes symmetrical with respect to the $Y = 0.5$, which lay on the center line of the torii's tubes. Indeed, the trajectory of a particle seeded in $(x_0, y_0, z_0) = (0.5, 0.255, 0.19)$ point is closed and rather thin, see Fig. 8. During the tracing, the maximum relative particle's deviation from $Y = 0.255$ plane was about 3%. This path lays inside all the ring torii formed by the liquid particles' trajectories.

Thus, the three-dimensional convective flow in an enclosure consists of the buoyancy-driven main cross-flow and secondary ones (relatively weaker than the main one) spreading from end-wall regions. The latter is a result of a coupling of the swirling convective flow and no-slip conditions on the lateral $Y = 0$, 1 walls.

It is worth noting that the described above flow regime can be observed only when the Grashof numbers are relatively small. In [Lappa (2005)], it was shown by means of three-dimensional computer simulations for $Pr = 0.01$ in a cube that for the Grashof number beyond 5×10^3 the cross-flow spreads from the endwalls into the entire bulk, and the flow has a more complicated structure. Even an unsteady regime could be observed.

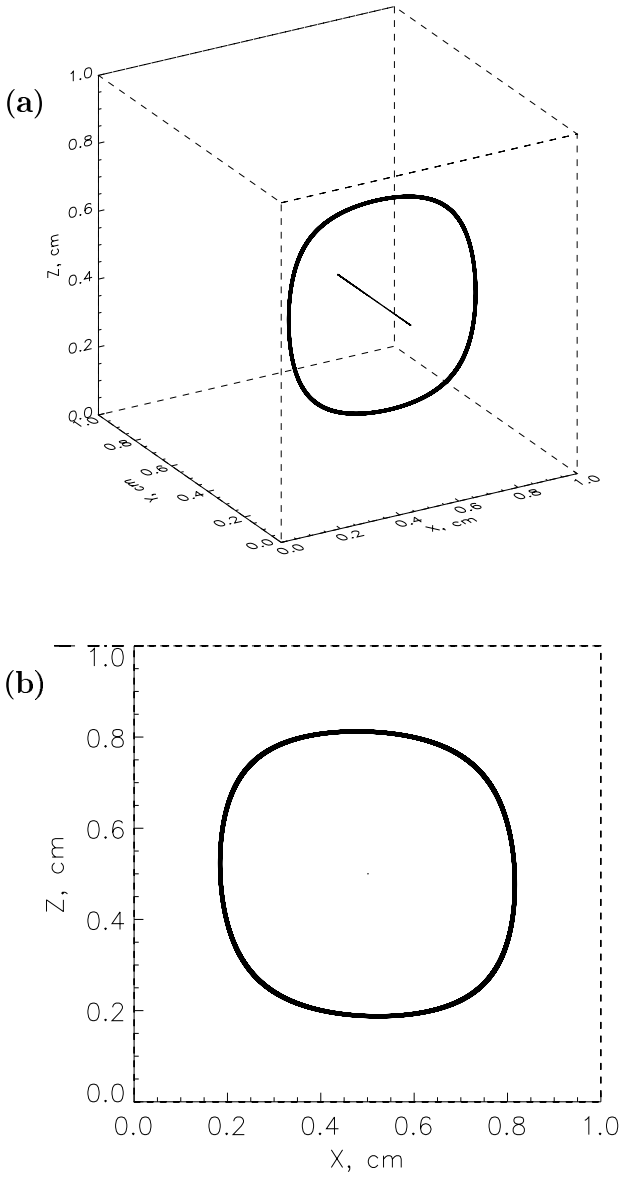

Figure 8 : Two liquid particles' trajectories traced for the 3D case by Method 3 seeded at $(x_0, y_0, z_0) = (0.5, 0.1, 0.5)$ and $(x_0, y_0, z_0) = (0.5, 0.255, 0.19)$. Two different views are shown. The former particle goes straightly to the cube's center (line) the latter follows rather thin closed trajectory (loop).

6 Conclusions

Buoyancy-driven convective flows have been studied in a cubic cell with differently heated opposite lateral walls. The steady flow patterns have been investigated by the liquid particle tracing technique. The study showed that accurate interpolation of velocity field at an arbitrary point from nodal points of computational grid plays a crucial role in precise particles' tracing. Results obtained by a combination of trilinear interpolation of velocity on the computational grid and eighth order Runge-Kutta algorithm are not satisfying for a long time-scale tracing. However, an initially performed resampling the velocity field by cubic spline interpolation on a new grid, approximately twice finer than the computational (before integrating the liquid particle's kinematic equations) results in accurate tracing. Even combined with a first order single time forward marching method, precise interpolation of velocity gives very accurate tracing.

Another finding of this research is a general incorrectness of modeling three-dimensional buoyancy-driven convective flow by two-dimensional approach. The larger the Prandtl number, the stronger the three-dimensionality is. Everywhere inside the cubic cell the liquid flow deviates from the analogous two-dimensional. Moreover, in the three-dimensional case the liquid particles' trajectories in the mid-plane are not closed circles.

Three-dimensional flow is organized so that in the mid-plane, where the perpendicular velocity is zero, the liquid performs spiral-type movement outwards, which is caused by the flow beyond this plane. The particles on the both sides with respect to the mid-plane make thin closed spiral trajectories forming ring torii-like surfaces in space. Flowing upward along the hot face and downward along the cold, the liquid particles are subjected to an additional movement in the perpendicular direction: drifting outward on the outer surfaces of the torii, and in the opposite direction along the inner torii's surfaces. The liquid flows noticeably faster when drifting toward the mid-plane and thus it is involved in a shuttle-like flow between the lateral walls and the mid-plane.

References

Blet, V.; Berne, P.; Chaussy, C.; Perrin, S.; Schweich, D. (1999): Characterization of a packed column using radioactive tracers. *Chemical Engineering Science*, vol. 54, pp. 91–101.

Cabral, B.; Leedom, C. (1993): Imaging vector fields using line integral convolution. *Computer Graphics (SIGGRAPH 93 Proceedings)*, pp. 263–270.

Crawfis, R.; Max, N. (1993): Texture splats for 3d scalar and vector field visualization. *Proc. IEEE Visualization*, pp. 261–265.

Davis, S. H. (1967): Convection in a Box: Linear Theory. *J. Fluid Mech.*, vol. 30, pp. 465–478.

Fletcher, C. A. J. (1988): *Computational Techniques for Fluid Dynamics*. Springer-Verlag, Berlin.

Gelfgat, A. Y. (1999): Different Modes of RayleighBénard Instability in Two- and Three-Dimensional Rectangular Enclosures. *Journal of Computational Physics*, vol. 156, no. 2, pp. 300–324.

Gingold, R. A.; Monaghan, J. J. (1977): Smoothed particle hydrodynamics, theory and application to non-spherical stars. *Mon. Nat. R. Astr. Soc.*, vol. 181, pp. 375–389.

Goode, D. J.; Konikow, L. F. (1989): Modification of a method of characteristics solute transport model to incorporate decay and equilibrium-controlled sorption and ion exchanges. *U.S. Geological Survey Water-Resources Investigations Report 89-4030*.

Helman, J. L.; Hesselink, L. (1991): Visualizing vector field topology in fluid flows. *IEEE Computer Graphics and Applications*, vol. 11, no. 3, pp. 36–46.

Hiller, W. J.; Koch, S.; Kowalewski, T. A.; de Vahl Davis, G.; Behnia, M. (1990): Experimental and numerical investigation of natural convection in a cube with two heated side walls. *Topological Fluid Mechanics*, pp. 717–726.

Hiller, W. J.; Koch, S.; Kowalewski, T. A.; Stella, F. (1993): Onset of natural convection in a cube. *Intl. J. Heat Mass Transfer*, vol. 13, pp. 3251–3263.

Hultquist, J. P. M. (1990): Interactive numerical flow visualization using stream surfaces. *Computing Systems in Engineering*, vol. 1, no. 2-4, pp. 349–353.

Johnson, A. A.; Tezduyar, T. E. (1997): 3D Simulation of Fluid-Particle Interactions with the Number of Particles Reaching 100. *Computer Methods in Applied Mechanics and Engineering*, vol. 145, pp. 301–321.

Lane, D. A. (1996): Visualizing Time-Varying Phenomena In Numerical Simulations Of Unsteady Flows. , no. NAS-96-001.

Lappa, M. (2005): On the nature and structure of possible three-dimensional steady flows in closed and open parallelepipedic and cubical containers under different heating conditions and driving forces. *FDMP*, vol. 1, no. 1, pp. 1–20.

Lu, N. (1994): A semi analytical method of path line computation for transient finite-difference groundwater flow models. *Water Resources Research*, vol. 30, no. 8, pp. 2449–2459.

Mallinson, G. D.; de Vahl Davis, G. (1977): Three-dimensional natural convection in a box: a numerical study. *J. Fluid Mech.*, vol. 83, pp. 1–31.

Nielson, G. M.; Magen, M.; Müller, H. (1997): *Scientific visualization overviews, methodologies, techniques*. IEEE Computer Society Los Alamitos.

Oñate, E.; Idelsohn, S. R.; Zienkiewicz, O. C.; Taylor, R. L. (1966): A finite point method in computational mechanics, application to convective transport and fluid flow. *Intl. J. Numer. Methods Eng.*, vol. 39, pp. 3839–3866.

Post, F. H.; Walsum, T. V. (1993): Fluid flow visualization. *Focus on Scientific Visualization, H. Hagen, H. Müller, G.M. Nielson (eds.)*, pp. 1–40.

Raffel, M.; Willert, C.; Kompenhaus, J. (1997): *Particle Image Velocimetry*. Springer-Verlag, Berlin.

Rybak, O.; Huybrechts, P. (2003): A comparison of Eulerian and Lagrangian methods for dating in numerical ice-sheet models. *Annals of Glaciology*, vol. 37, pp. 150–158.

Shafer, J. M. (1987): Reverse pathline calculation of time-related capture zones in nonuniform flow. *Ground Water*, vol. 25, no. 3, pp. 283–289.

Shevtsova, V. M.; Melnikov, D. E.; Legros, J. C. (2001): Three-dimensional simulations of hydrodynamical instability in liquid bridges. Influence of temperature-dependent viscosity. *Phys. Fluids*, vol. 13, pp. 2851–2865.

Shevtsova, V. M.; Melnikov, D. E.; Legros, J. C. (2004): The study of oscillatory weak flows in space experiments. *Microgravity Sci. Technol.*, vol. XV, no. 1, pp. 49–61.

Tarver, D. S.; Plant, G. R. (1995): Case report: the effect of contrast density on computed tomographic arterial portography. *Br. J. Radiol.*, vol. 68, pp. 200–203.